Supporting Information

Sequential Multiple-Target Sensor: In^{3+}, Fe^{2+} and Fe^{3+} Discrimination by an Anthracene-Based Probe

Alba Finelli [†], Valentin Chabert [†], Nelly Hérault [†], Aurélien Crochet [‡], Cheal Kim[#], Katharina M. Fromm [,†]*

[†] Department of Chemistry, University of Fribourg, Ch. du Musée 9, 1700 Fribourg, Switzerland

[‡] FriMat, Department of Chemistry, University of Fribourg, Ch. du Musée 9, 1700 Fribourg, Switzerland

[#]Department of Fine Chemistry, Seoul National University of Science and Technology (SeoulTech), Seoul 139-743, Republic of Korea

Table of Contents

General

All chemicals were commercial products of reagent grade and were used without further purification. ^{1}H and ^{13}C NMR measurements were carried out with a Bruker 400 MHz spectrometer at ambient temperature, and chemical shifts are given in ppm with respect to the residual solvent peak. Mass spectra (ESI-TOF, positive mode) were recorded with a Bruker esquire HCT spectrometer with a DMF/ACN mixture as solvent. The UV-vis spectra were recorded with a Perkin–Elmer Lambda 40 spectrometer. The crystallographic data of single crystals were collected with Mo-K_{α} radiation (λ = 0.71073 Å). All measurements were performed at 200 K, with Stoe IPDS-II or IPDS-II T diffractometers equipped with Oxford Cryosystem open-flow cryostats. Single crystals were picked under the microscope, and placed in inert oil. All crystals were mounted on loops and all geometric and intensity data were taken from one single crystal. The absorption corrections were partially integrated in the data reduction procedure. The structures were solved and refined using full-matrix least-squares on F^2 with the SHELX-2014 package. All atoms (except hydrogen atoms) were refined anisotropically. Hydrogen atoms were refined where possible, and otherwise added using the riding model position parameters.

NMR Spectra of S1' and S1

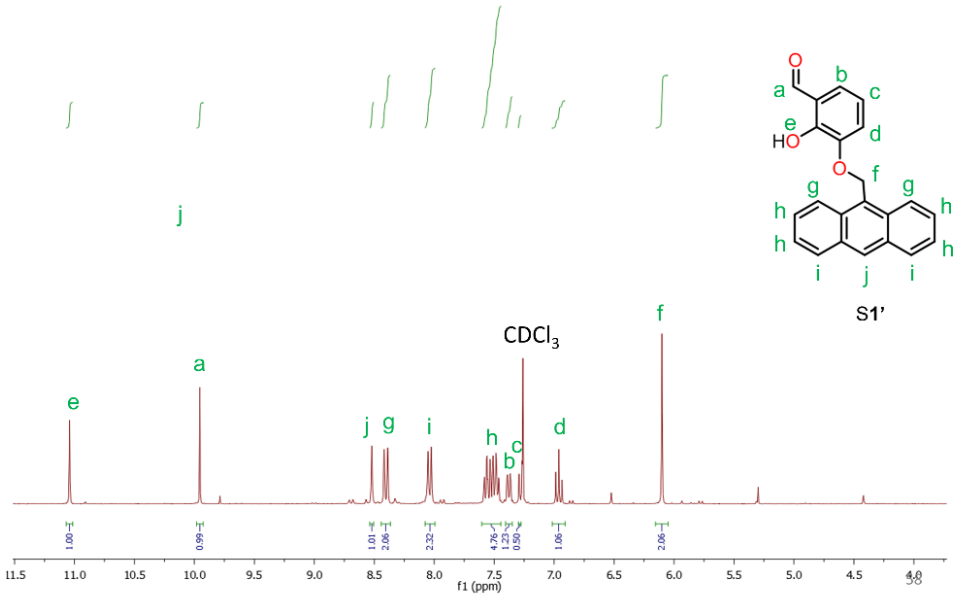

Figure S1: ^{1}H NMR spectrum of the precursor **S1'** in $CDCl_3$**.**

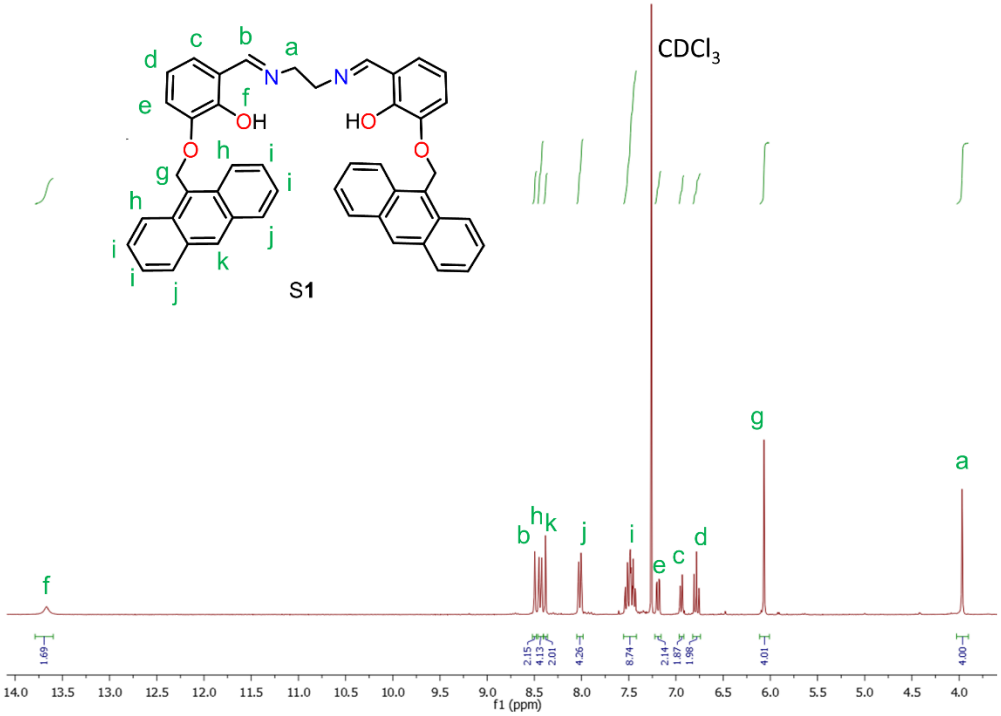

Figure S2: ^{1}H NMR spectrum of the anthracene-based ligand **S1** in $CDCl_3$.

Fe^{2+} and Fe^{3+} Oxidation Test

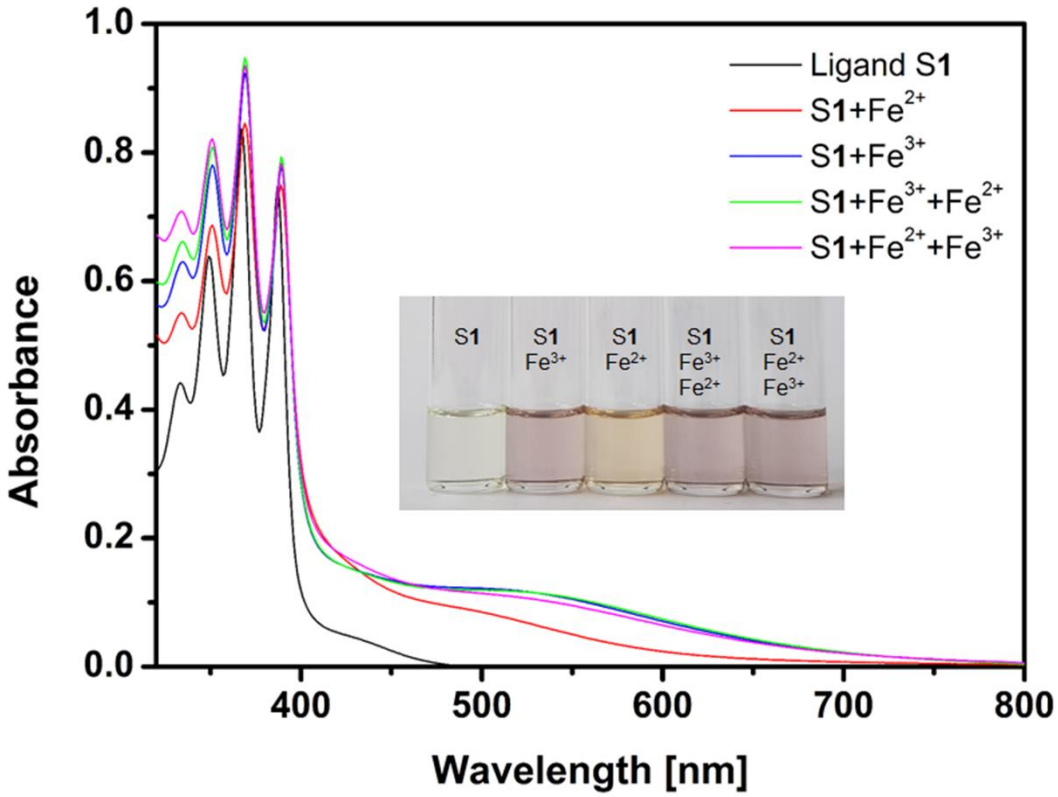

Figure S3: UV-Vis spectra of **S1** (40 µM) solutions containing Fe^{2+} and/or Fe^{3+} salts under degassed conditions.

UV-Vis Titration of sensor S1

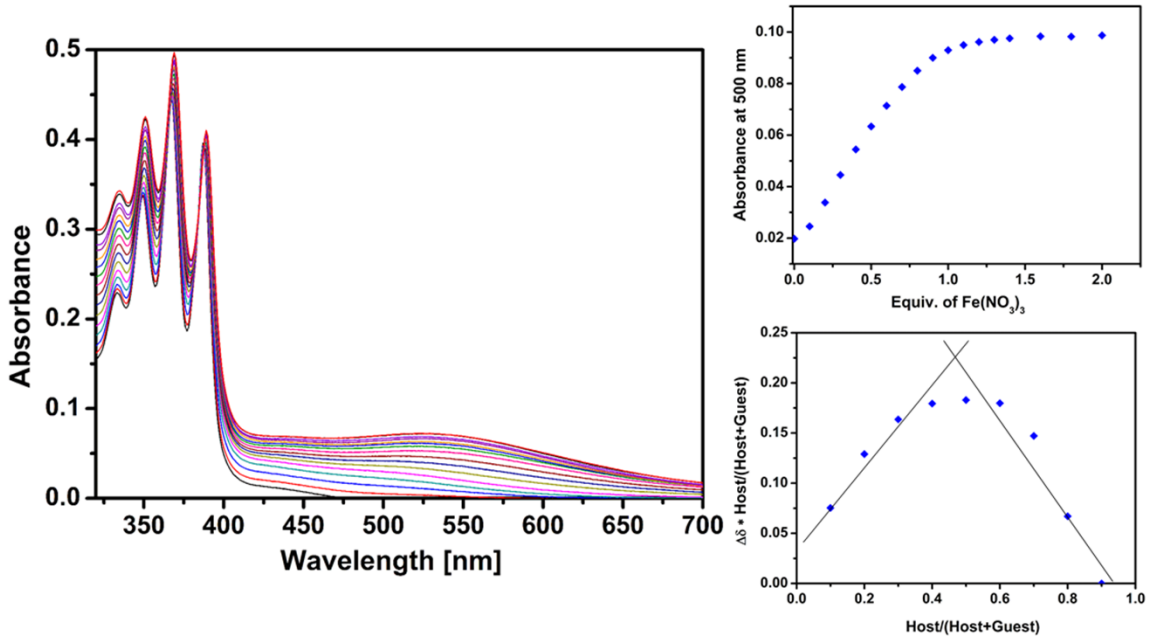

Figure S4: Titration of ligand **S1** (40 µM) with $Fe(NO_3)_3$, the corresponding binding isotherm curve and the Job Plot.

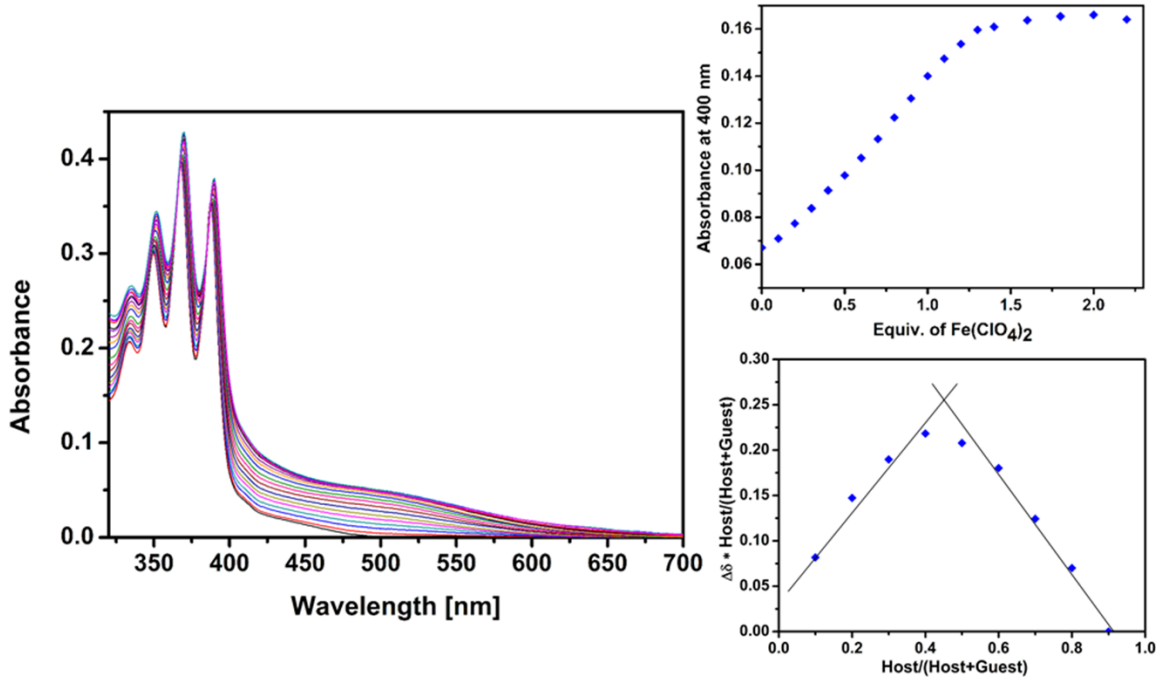

Figure S5: Titration of ligand **S1** (40 µM) with $Fe(ClO_4)_2$, the corresponding binding isotherm curve and the Job Plot.

ESI mass analysis for Fe^{3+} complex

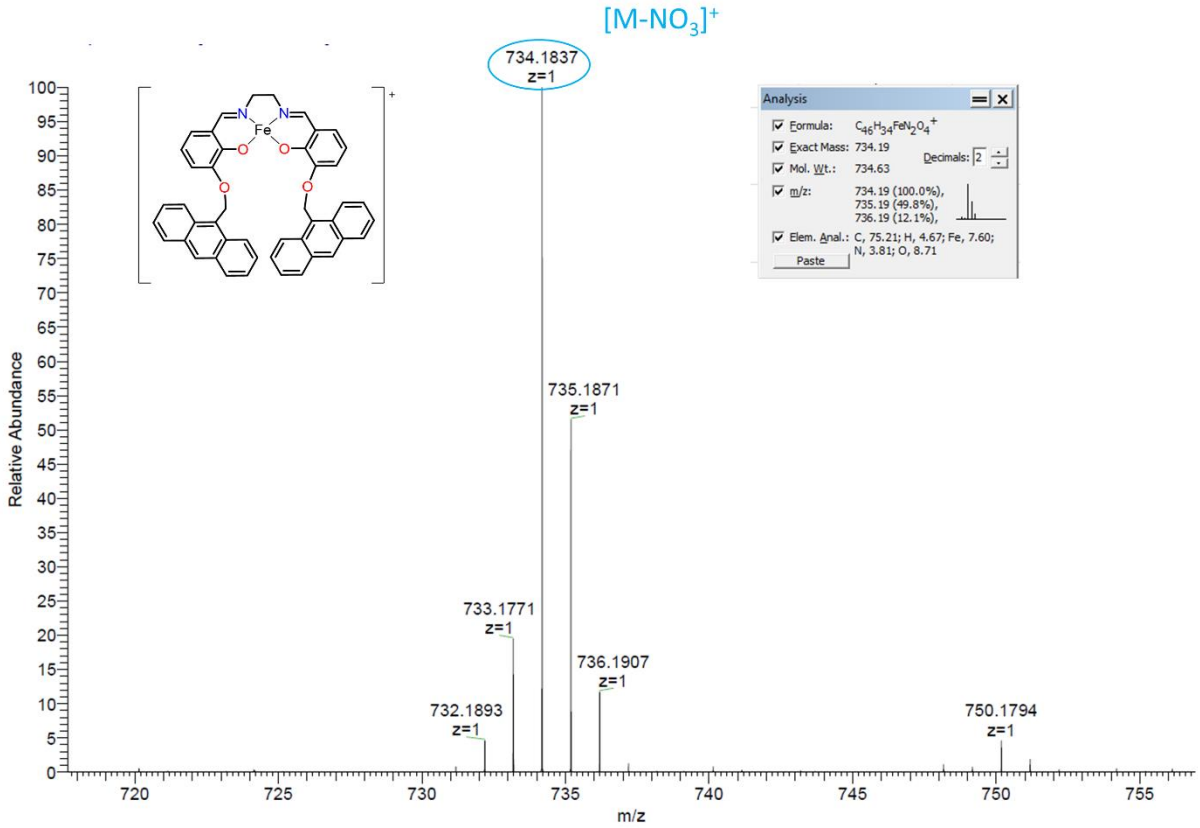

M([Fe**S1**-2H)+NO_3)]) = 796.12

Figure S6: ESI-MS analysis of the Fe^{3+}-**S1** complex.

NMR Titration of the Probe S1 with Fe^{3+} and Fe^{2+}

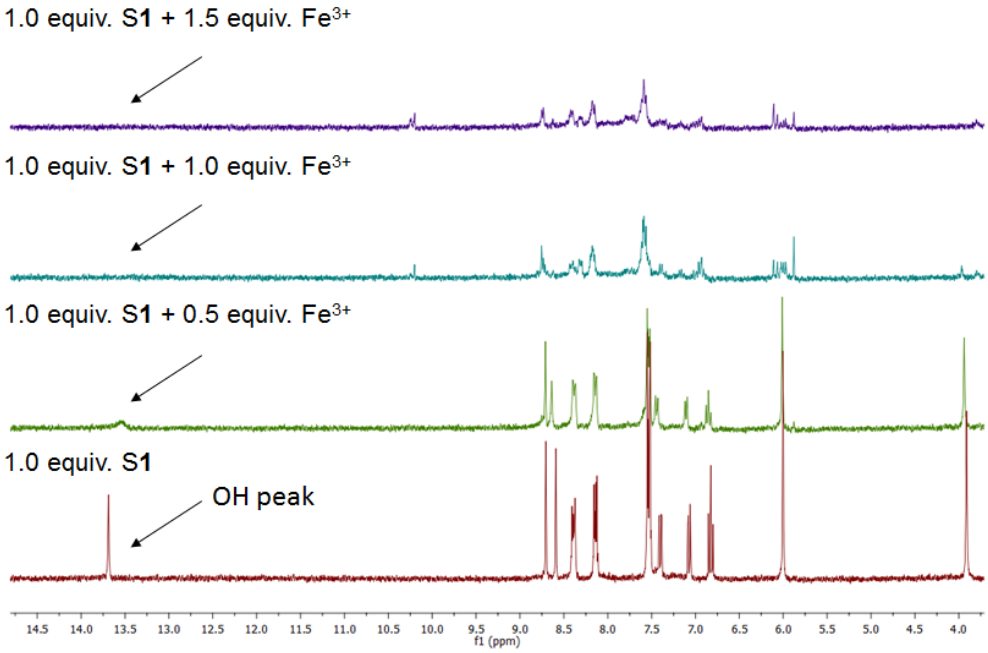

Figure S7: NMR titration of the ligand **S1** (1mM) with $Fe(NO_3)_3$ in DMSO.

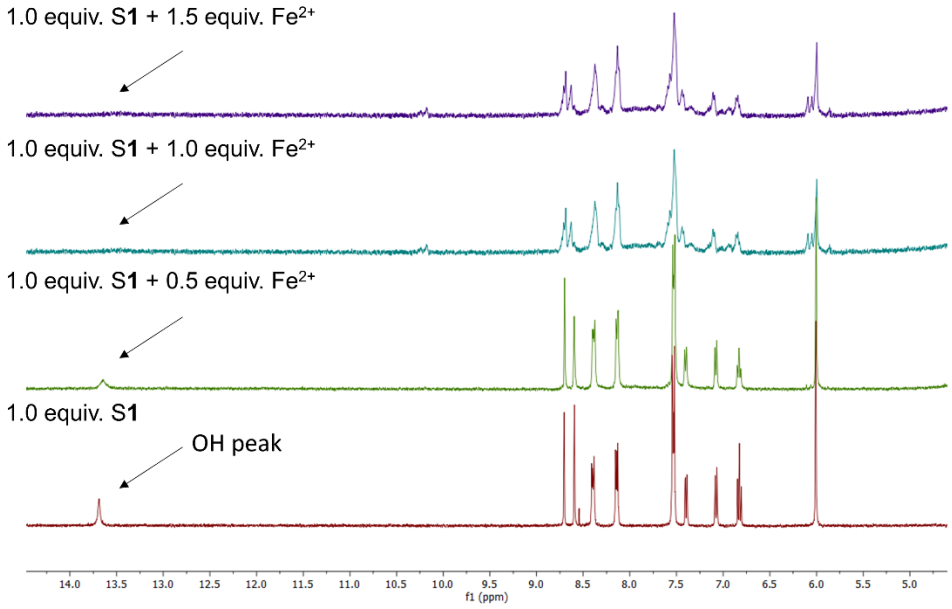

Figure S8: NMR titration of the ligand **S1** (1 mM) with $Fe(ClO_4)_2$ in DMSO.

Detection limit of Fe^{2+} and Fe^{3+}

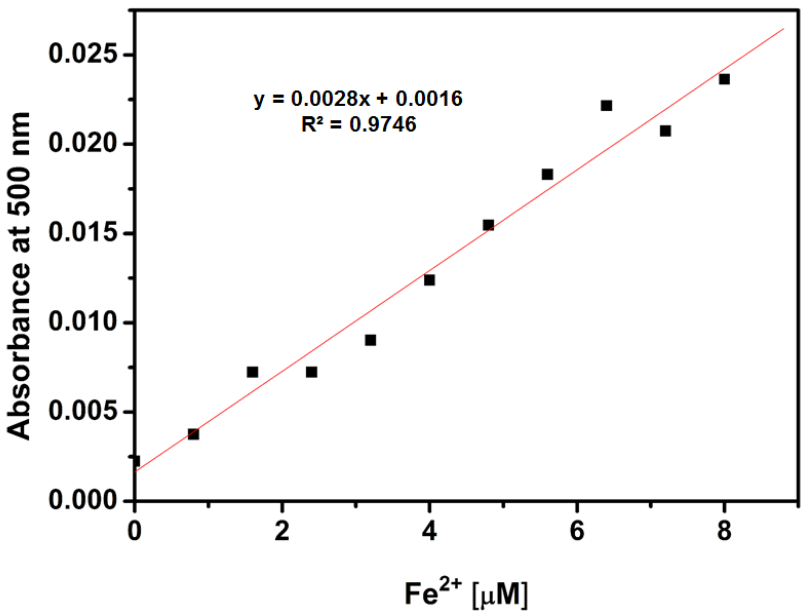

Metal concentration (μM)	Intensity	y =(a*Conc.)+b	Variance	Standard deviation
0	0.00225	0.0016	4.225E-07	0.00065
0.8	0.00375	0.00384	8.1E-09	9E-05
1.6	0.00723	0.00608	1.3225E-06	0.00115
2.4	0.00723	0.00832	1.1881E-06	0.00109
3.2	0.00903	0.01056	2.3409E-06	0.00153
4	0.01239	0.0128	1.681E-07	0.00041
4.8	0.01546	0.01504	1.764E-07	0.00042
5.6	0.01831	0.01728	1.0609E-06	0.00103
6.4	0.02216	0.01952	6.9696E-06	0.00264
7.2	0.02074	0.02176	1.0404E-06	0.00102
8	0.02364	0.024	1.296E-07	0.00036

σ Value (average of standard deviation)**:** 0.000944545

L.O.D ((3*σ)/a)**:** 0.69113082 μM

Figure S9: Standard deviations and linear fitting for detection limit calculations of **S1** (40 μM) + Fe^{2+}.

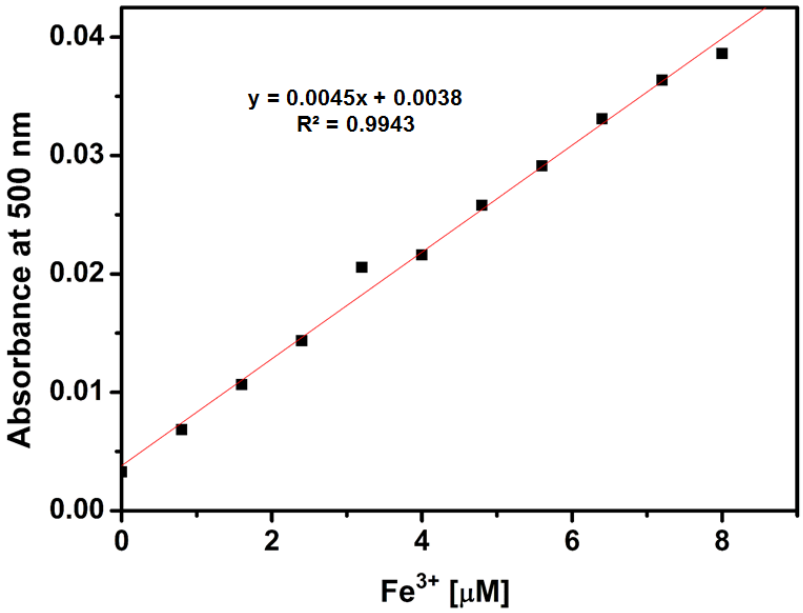

Metal concentration (μM)	Intensity	y =(a*Conc.)+b	Variance	Standard deviation
0	0.00327	0.0038	2.809E-07	0.00053
0.8	0.00685	0.0074	3.025E-07	0.00055
1.6	0.01066	0.011	1.156E-07	0.00034
2.4	0.01436	0.0146	5.76E-08	0.00024
3.2	0.02057	0.0182	5.6169E-06	0.00237
4	0.0216	0.0218	4E-08	0.0002
4.8	0.0258	0.0254	1.6E-07	0.0004
5.6	0.02913	0.029	1.69E-08	0.00013
6.4	0.0331	0.0326	2.5E-07	0.0005
7.2	0.03637	0.0362	2.89E-08	0.00017
8	0.03862	0.0398	1.3924E-06	0.00118

σ Value (average of standard deviation)**:** 0.000600909

L.O.D ((3*σ)/a)**:** 0.439689579μM

Figure S10: Standard deviations and linear fitting for detection limit calculations of **S1** (40 μM) + Fe^{3+}.

Fluorescent Titration of sensor S1

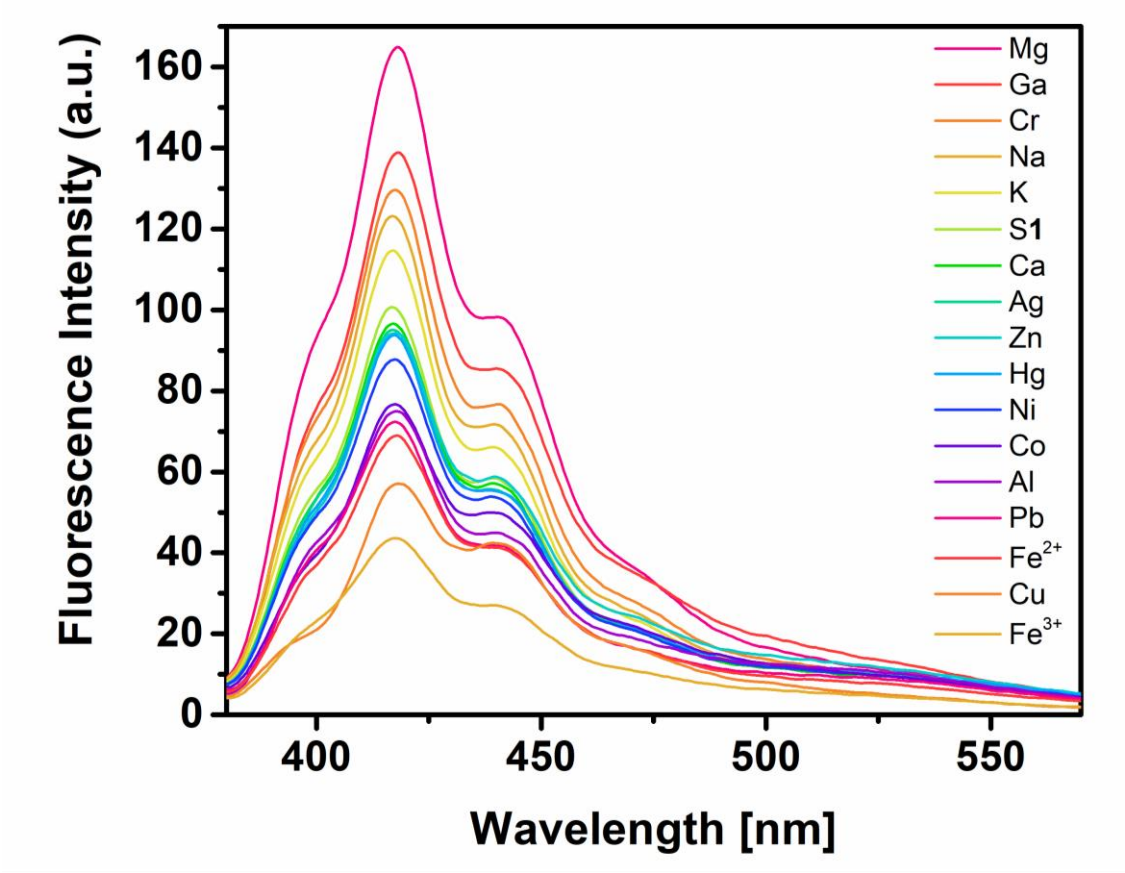

Figure S11: Fluorescence intensity variation depending on the metal ion used. The fluorescence emission spectra (λ_{ex} = 365 nm) of **S1** (40 μM in DMF) were obtained after the addition of 1.2 equiv. of different metal ions (Ag^{+}, Al^{3+}, Ga^{3+}, Zn^{2+}, Cu^{2+}, Mg^{2+}, Cr^{3+}, Co^{2+}, Ni^{2+}, Na^{+}, K^{+}, Ca^{2+} and Pb^{2+}).

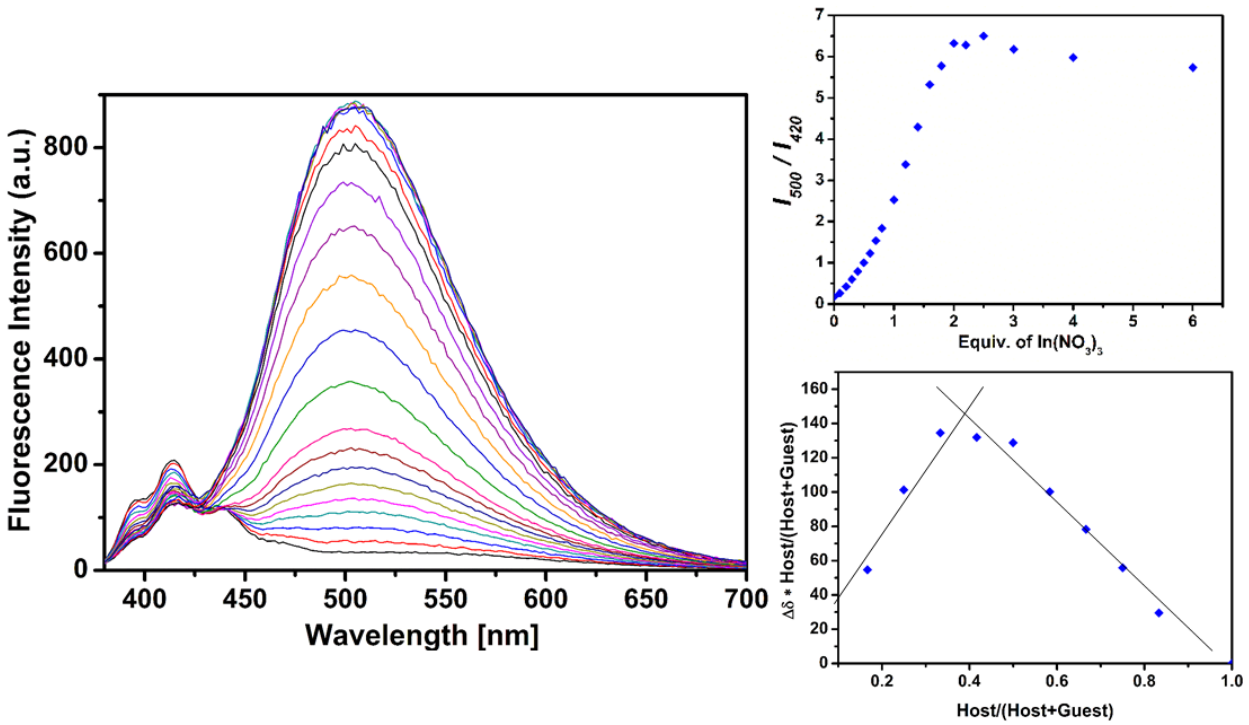

Figure S12: Titration of ligand **S1** (40 µM) with $In(NO_3)_3$, the corresponding binding isotherm curve and the Job Plot.

Detection limit of In^{3+}

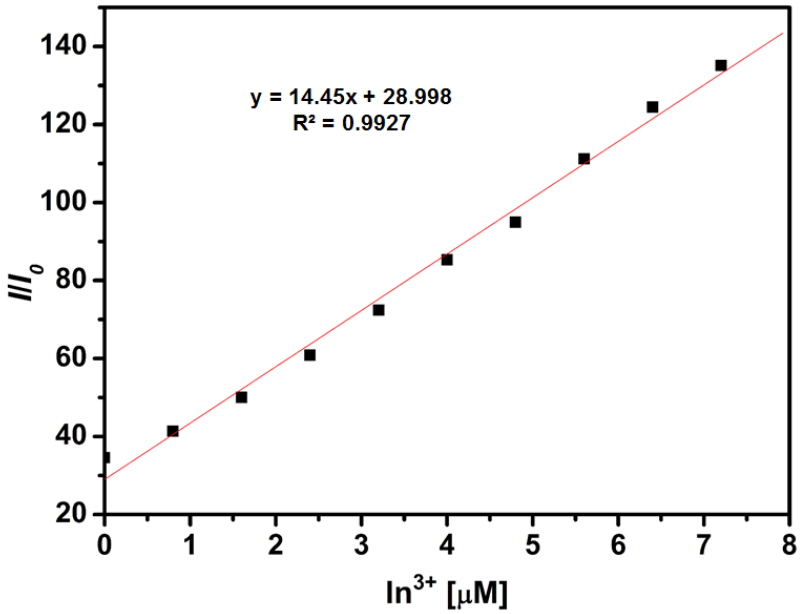

Metal concentration (μM)	Intensity	y =(a*Conc.)+b	Variance	Standard deviation
0	34.57075119	28.998	31.05555583	5.57275119
0.8	41.38391495	40.558	0.682135505	0.82591495
1.6	50.03685379	52.118	4.331169547	2.08114621
2.4	60.7942009	63.678	8.316297249	2.8837991
3.2	72.40631866	75.238	8.018419211	2.83168134
4	85.26144409	86.798	2.361004065	1.53655591
4.8	94.96090698	98.358	11.54024099	3.39709302
5.6	111.2199631	109.918	1.695107914	1.3019631
6.4	124.4255447	121.478	8.688019758	2.9475447
7.2	135.1032257	133.038	4.265157192	2.0652257

σ Value (average of standard deviation)**:** 2.544367522

L.O.D ((3*σ)/a)**:** 0.528242392 μM

Figure S13: Standard deviations and linear fitting for detection limit calculations of **S1** (40 μM) + In^{3+}.

ESI mass analysis for In^{3+} complex

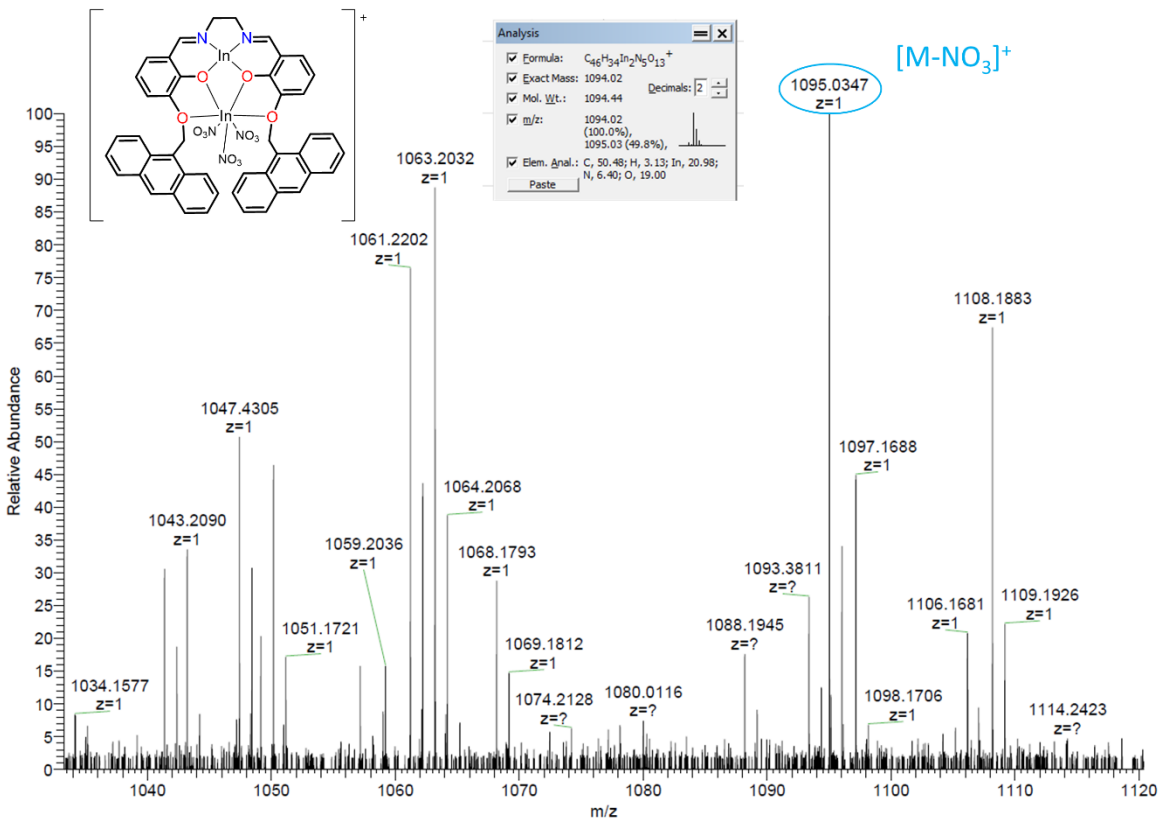

M([(In_2**S1**-2H)+4NO_3]) = 1156.03

Figure S14: ESI-MS analysis of the In^{3+}-**S1** complex.

Fluorescence emission spectrum of InS1 complex in $CHCl_3$/MeOH

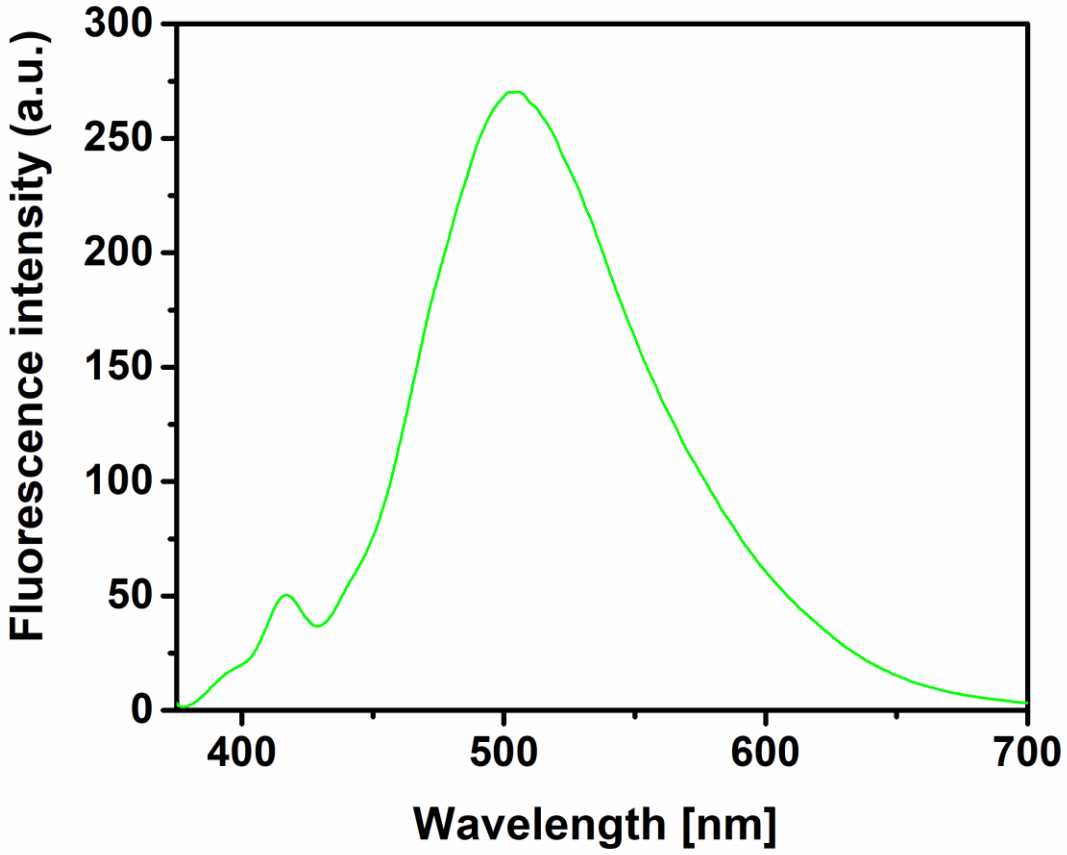

Figure S15: Fluorescence emission spectrum (λ_{ex} = 365 nm) of **S1** (40 μM) in $CHCl_3$ in presence of 3 equiv. of $In(NO_3)_3$ (in DMF).

NMR Titration of the Probe S1 with In^{3+}

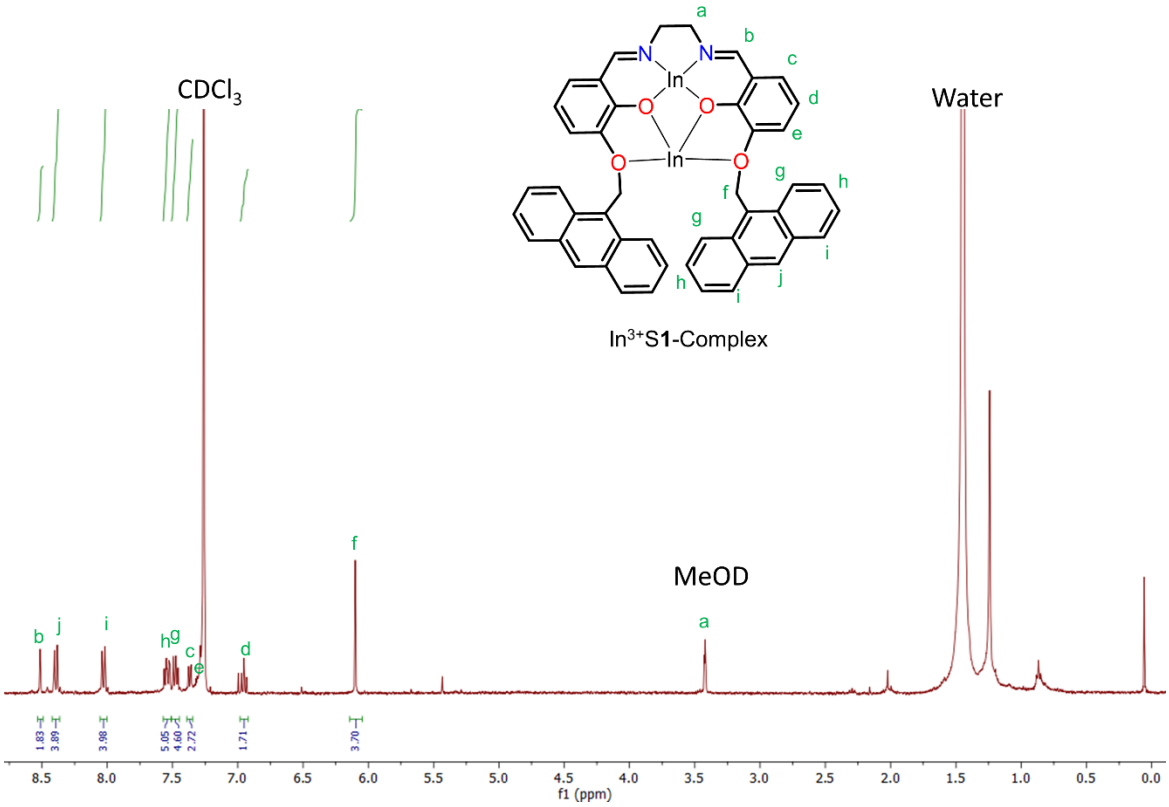

Figure S16: ^{1}H NMR spectrum of the In^{3+}-**S1** complex in $CDCl_3$.

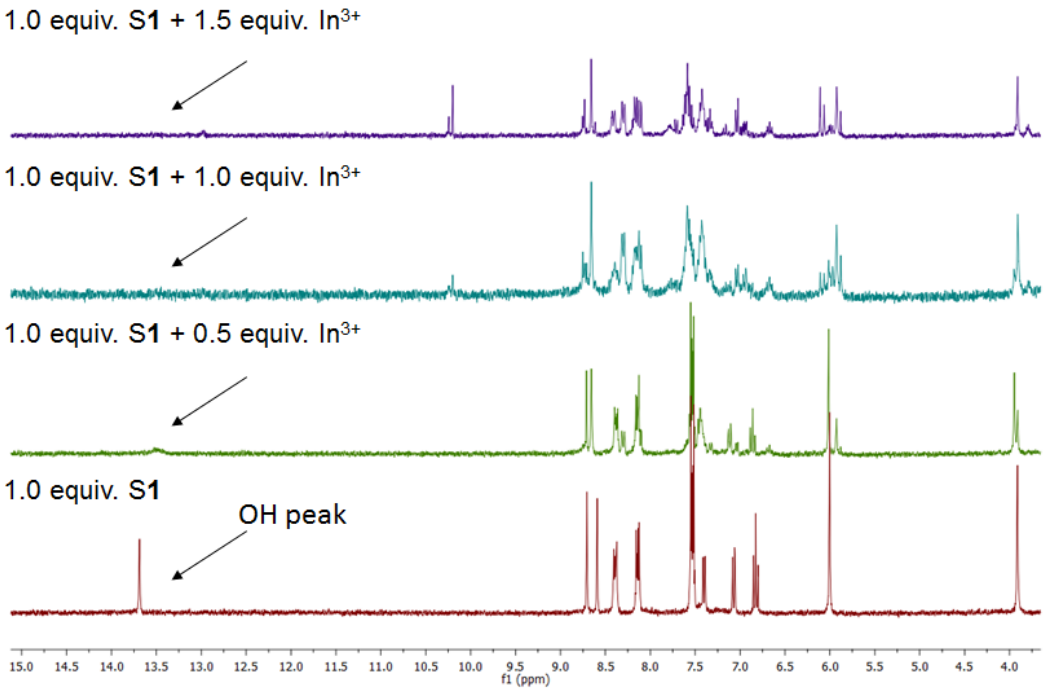

Figure S17: NMR titration of the ligand **S1** (1mM) with $In(NO_3)_3$ in DMSO.

Competition Experiments

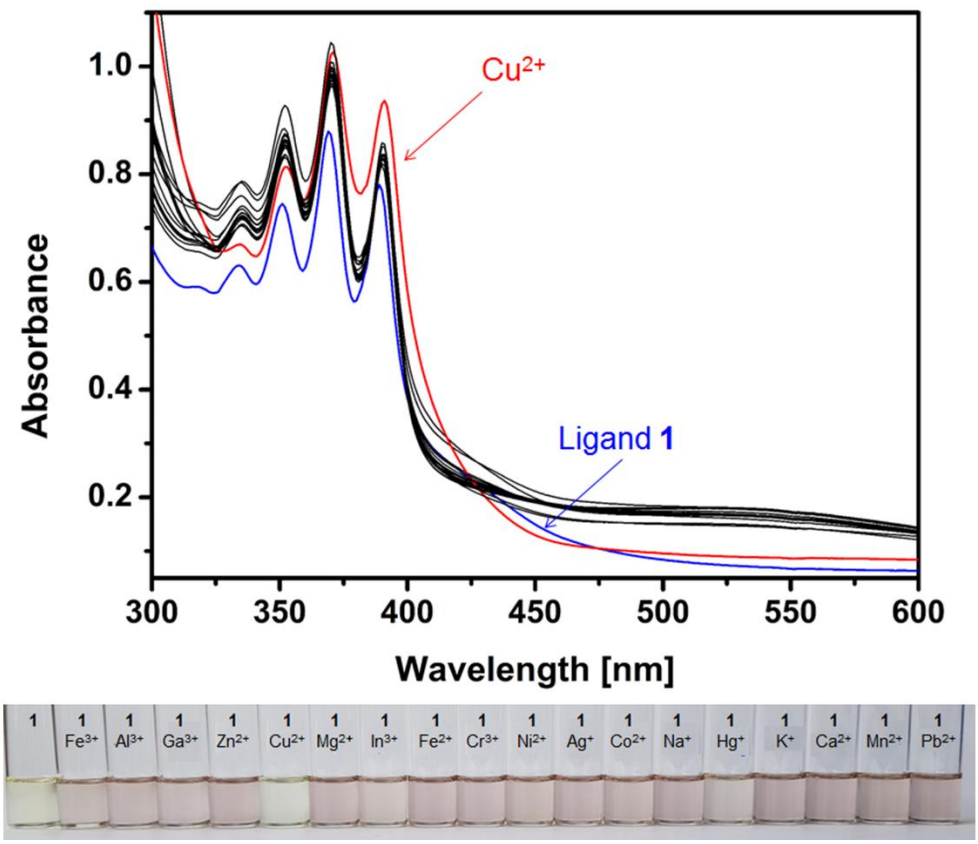

Figure S18: UV-Vis spectra of **S1** solutions (40 µM) containing equimolar concentrations (48 µM) of Fe^{3+} and foreign metal ions.

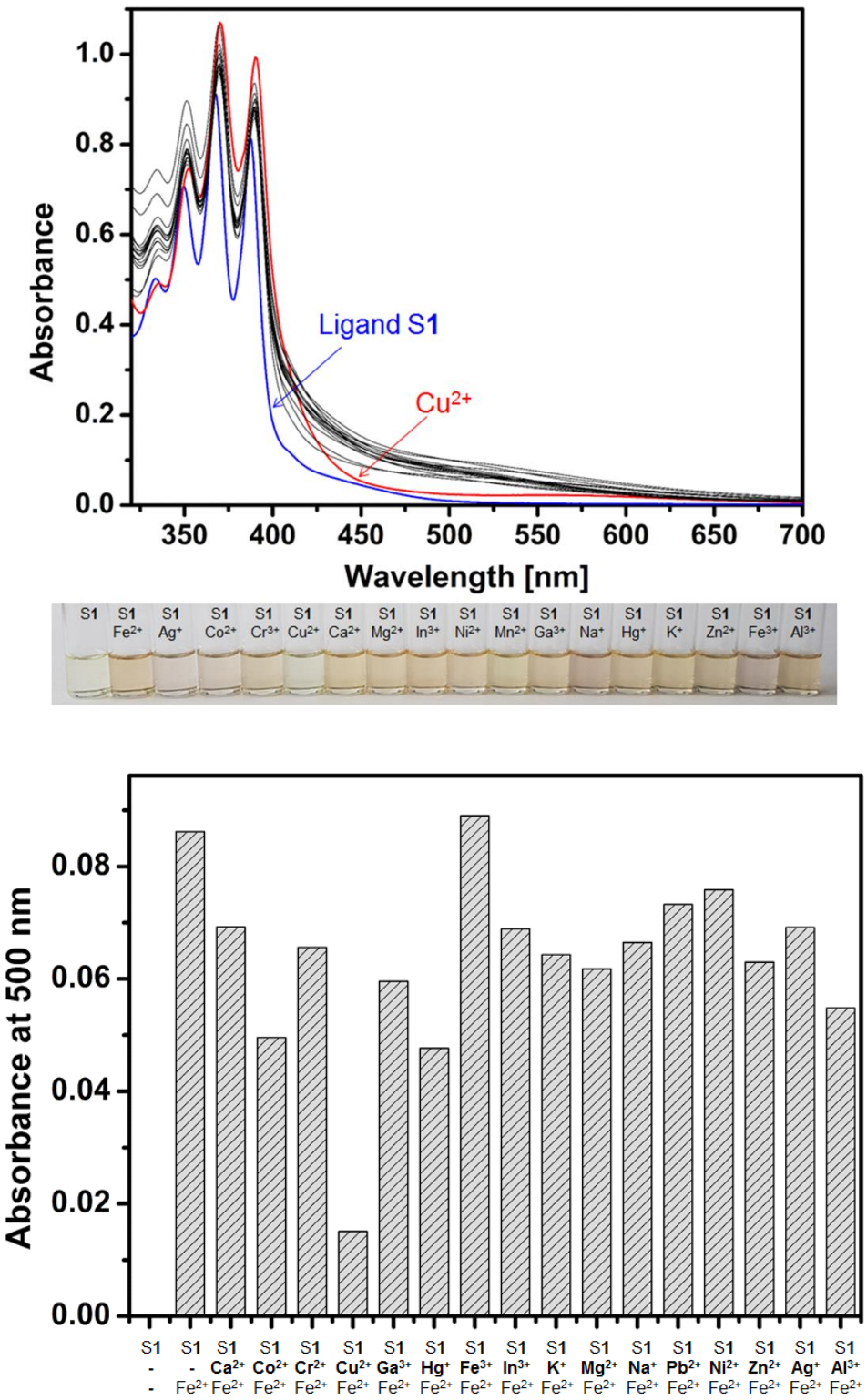

Figure S19: UV-Vis spectra of **S1** solutions (40 µM) containing equimolar concentrations (48 µM) of Fe^{2+} and foreign metal ions.

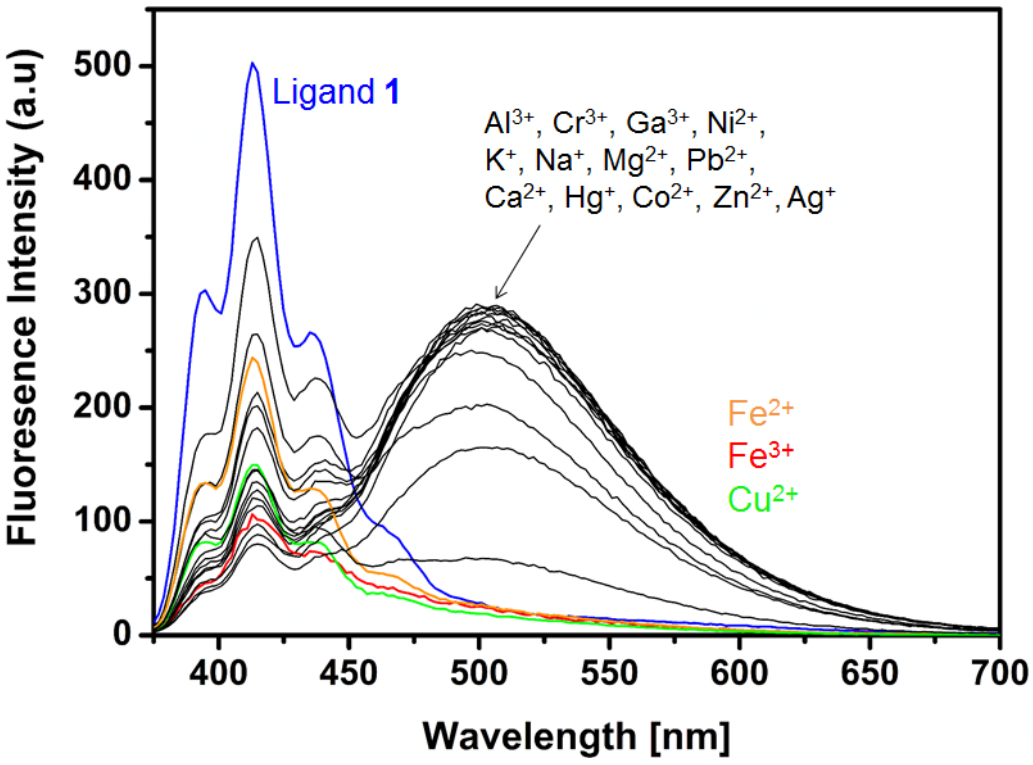

Figure S20: UV-Vis spectra of **S1** solutions (40 µM) containing equimolar concentrations (88 µM) of In^{3+} and foreign metal ions.

UV-Vis sensor S1 with Cu^{2+}

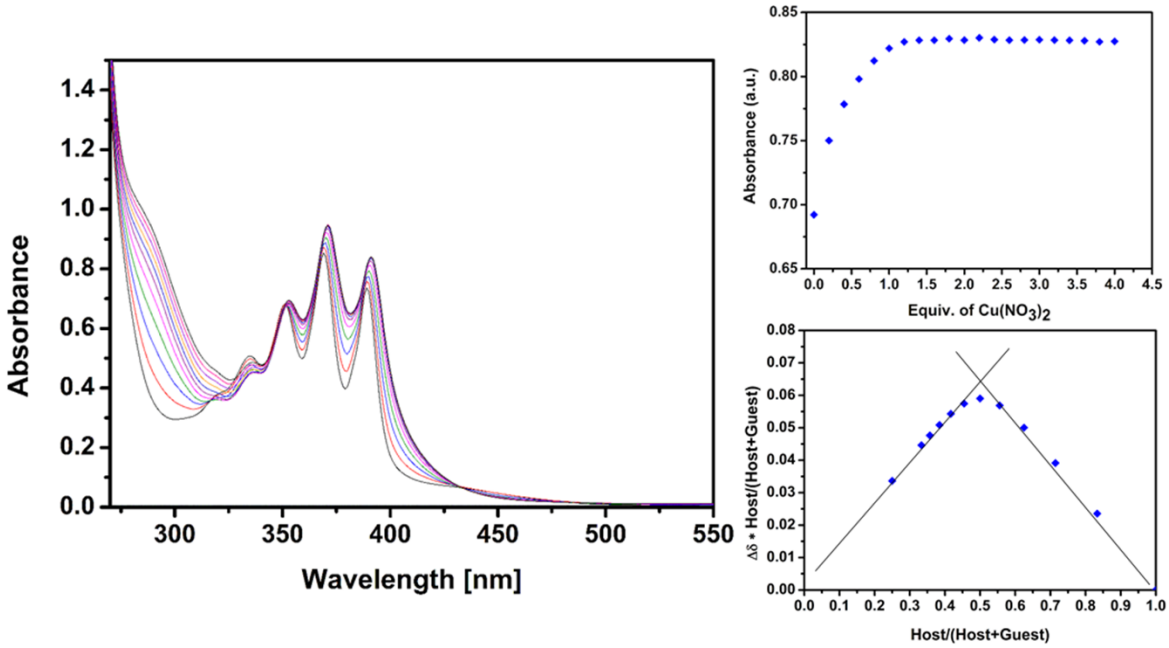

Figure S21: Titration of ligand **S1** (40 µM) with $Cu(NO_3)_2$, the corresponding binding isotherm curve and the Job Plot.

Crystallography

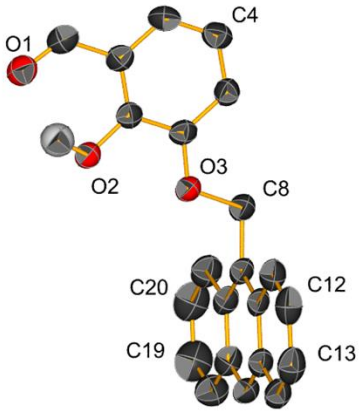

Figure S22: Crystal structure of anthracene-based aldehyde **S1'**, all H-atoms are omitted for clarity (thermal ellipsoids at 50 % probability level).

Sensor S1

Sensor **S1** crystallized in the orthorhombic *P*ccn space group (N°56), as yellow block-like crystals by slow evaporation in DCM. Completely symmetric, the external anthracene moieties are nearly perpendicular to the benzene ring planes with an angle of 85.09°. The two side arms of the sensor are repelled to each other in an anti-parallel arrangement with an angle of 70.36° due to the steric hindrance of the two chromophores. This arrangement is stabilized by the H-bond between the alcohol group protons H1 and the N-atom, N1, with a distance of 1.947 Å. While C21–π, π–C1#4 and C18–C13#4 interactions (3.431 Å, 3.792 Å and 3.632 Å, respectively) allows an expansion of the structure into the direction of the *c*-axis, a growth along the *a*-axis is governed by the C20–C9#6 contact (3.342 Å).

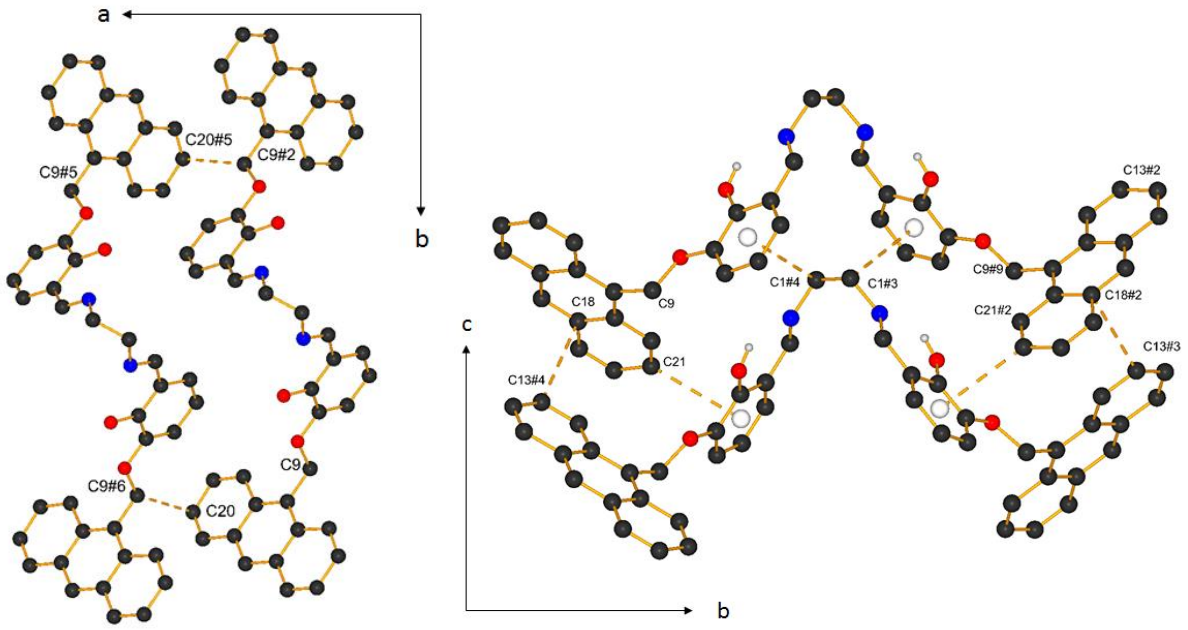

Figure S23: Crystal structure of sensor **S1** (#2(1/2-x, ½-y, z), #3(x, ½-y, -1/2+z), #4(1/2-x, y, -½+z), #5(3/2-x, ½-y, z), #6(1+x, y, z)), all H-atoms are omitted for clarity, except for OH groups.

Complex Cu^{2+}-S1

Cu^{2+}-**S1** crystallized in a monoclinic space group *C*2/c (N° 15) in red plate-like crystals by slow diffusion of diethyl ether in a solution of the complex in THF. The Cu^{2+} cation occupied the N_2O_2 chelating site of the ligand **S1** in a quasi-perfect square planar fashion, formed by the phenolate moieties and imine groups. Having an average bond valence sum of 1.99 provided by the N_2O_2 cavity of the sensor, Cu^{2+} does not need to complete its coordination sphere using additional solvent or anions entities. The angle sum around the metal ions within the recognition moiety is 360.85°, indicating the approximate planarity of this coordination. Compared to the precedent structure, the structure of one side arm of the complex is almost preserved with an angle of 79.40° between the extern anthracene moiety and the plane formed by the di-oxo-benzene ring. For the other extremity of the compound, the anthracene moiety meets practically face to face the benzene ring with an angle of 64.44° stabilized by C32–π and C10–C33 interactions (3.584 Å and 3.534 Å, respectively) inducing a slight distortion of the planarity of the N_2O_2 coordination of 20.03° based on the aromatic ring planes. The bond between the ether O-atom and the carbon (C15–O1) of the distorted side, connecting the benzene core to the anthracene moiety, was observed to be shorter than in the regular side (C32–O4) with a distance of 115.66 Å and 117.17 Å, respectively. The crystal packing reveals that the probe **S1** is packed to each other along the *c*-axis in an anti-parallel layer like assembly by C15–C13#2 interactions (3.387 Å) from the regular anthracene groups and by C22–C38#3 contacts (3.371 Å) from the distorted anthracene moieties along the *a*-axis.

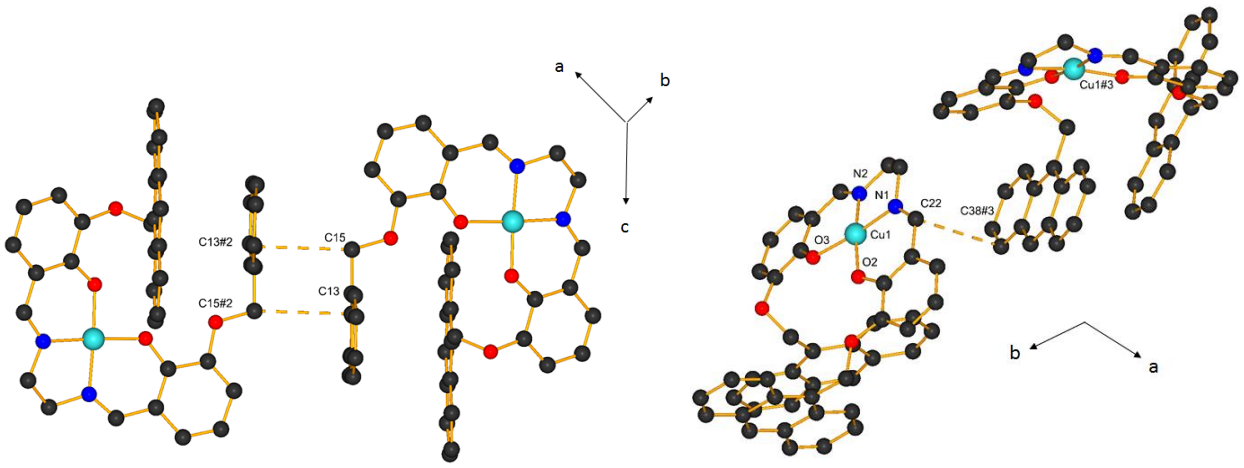

Figure S24: Crystal structure of the complex Cu^{2+}-**S1** (#2(1-x, 1-y, 1-z), #3(x, 2-y, 1/2+z)), all H-atoms are omitted for clarity.

Table S1: Crystallographic data.

	S1'	**S1**	**Cu^{2+}-S1**
Formula	$C_{22}H_{16}O_3$	$C_{46}H_{36}N_2O_4$	$C_{46}H_{34}CuN_2O_4$
M_w	328.35	680.77	742.29
T [K]	140	140	200
Lattice	Triclinic	Orthorhombic	Monoclinic
Space group	*P*-1	*P*ccn	*C*2/c
a [Å]	10.2229(6)	6.5460(10)	31.106(2)
b [Å]	17.9147(9)	45.378 (11)	12.6818(7)
c [Å]	18.2447(11)	11.5025(15)	22.0348(13)
α [°]	78.197(5)	90	90
β [°]	89.633(5)	90	125.843(4)
γ [°]	89.552(4)	90	90
V [$Å^3$]	3270.6(3)	3416.7(11)	7046.2(8)
Z	8	4	8
d_{calc} [g cm^{-3}]	1.334	1.323	1.399
R_1/ wR_2 *[I>2sigma(I)]*	0.0723/ 0.1963	0.1251/ 0.2762	0.0686/0.1523